

MATHEMATICAL ANALYSIS OF HOW SPINNING UNDER AN ANGLE AFFECTS THE VESTIBULAR SYSTEM OF PILOTS

Tsvetan Kachamachkov

8, Kl. Ohridski, Sofia, Bulgaria, TU-Sofia,
Postal Sofia - 1309, „Sv. Troitsa” 303 - B - 39

Abstract

One typical example of high-genus anatomical structures is called the vestibular system (VS) (see Figure 3). The VS is a genus-3 structure situated in the inner ear, which is a sensory structure responsible for detecting head movements and sending postural signals to the brain. The morphometry of VS plays an important role in the analysis of various diseases such as the Adolescent Idiopathic Scoliosis (AIS) disease. The AIS is a 3D spinal deformity which affects about 4% school children world wide. The etiology of AIS is still unclear but believed to be a multi-factorial disease. One popular hypothesis was suggested to be the structural changes in the VS that induce the disturbed balance perception, and further cause the spinal deformity. The morphometry of the VS becomes important to understand the disease.

- Mathematical analysis of how spinning under an angle affects the vestibular system of pilots.
- The author has made a mathematical analysis of how spinning under an angle affects the vestibular system of pilots.
- Achieving a thorough overview of mathematical analysis of how spinning under an angle affects the vestibular system of pilots.

1. INTRODUCTION

Zero gravity was a feature first introduced by NASA to explain what they found to be the optimal seating position for astronauts who were spending a good amount of their time strapped into their seat in their spaceship as it orbited the earth. This becomes apparent when you sit in a normal chair, with a normal horizontal seat and with a chair back that is either reclined or inclined, and then put the chair into a zero gravity position. If you focus on how your low back feels in both positions, you will become very aware of the additional “weight” or compression on the low back when the seat is horizontal. When the zero gravity positioning is introduced, you will suddenly become aware that the weight or compression on the low back shifts and now feels more evenly distributed throughout the whole body. The behaviour of the gyroscope is naturally described Figure 4. Schematic illustration of a MEMS implementation of the z-axis rate integrating gyroscope with respect to the non-inertial coordinate frame $\{x; y; z\}$. In this case, the governing equations in Cartesian coordinates $\{x; y; z\}$ are given by

$$X'' + \omega_n^2 X - 2\Omega Y' = 0 \quad (1)$$

$$Y'' + \omega_n^2 Y - 2\Omega X' = 0 \quad (2)$$

The essential feature of these equations is the presence of the Coriolis acceleration terms $-2\Omega Y'$ and $-2\Omega X'$. It is the Coriolis acceleration that causes a transfer of energy between the two gyro-

scope modes of operation. The resultant Coriolis force is perpendicular to both the input rate and the instantaneous radial velocity in the drive direction. This produces a motion of the proof mass in direction perpendicular to its initial oscillation. To measure rotation rate, the proof-mass is driven to a fixed amplitude along the x-axis by applying an electrostatic drive force to the proof-mass along the x-axis. In the absence of rotation there will be no motion of the proof-mass along the y-axis, (a). Under rotation, however, the Coriolis acceleration will cause energy to be transferred from the x-axis (primary mode) to the y-axis (secondary mode) building up a vibration amplitude along the y-axis. The ratio of the amplitude in the secondary mode of vibration to the amplitude of the primary mode of vibration can be shown to be proportional to the rotation rate and is given by [1]

$$\frac{Y}{X} = 2Q \frac{\Omega}{\omega_n} \quad (3)$$

Pilots have more developed vestibular system because of the constantly changing angle between 0 degree and 45 degree. There are some theories that spinning a human under this circumstances will help him develop a stronger and more evolved vestibular system. However there is no proof of these theories, which is one of the provocations for such a mathematical model and further studies in the field how spinning under different angles affects our vestibular system. 45 degree is not cho-

sen by a coincidence at this particular angle most of the pilot simulations work. Creating a mathematical model of these particular circumstances could be the key to unlocking the hidden human potential and developing our vestibular systems even farther. Maybe math will reveal the hidden secrets of the human vestibular system. I hope that number will answer that which has left the medicine speechless.

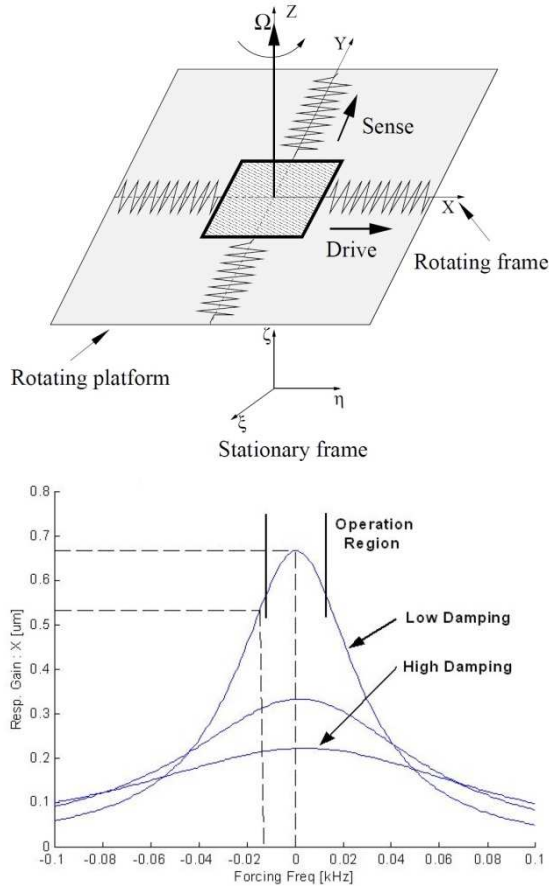


Figure 1. (a) Mass-spring model of the vibratory micromachined gyroscope; (b) The response of the vibratory gyroscope to the Coriolis force. [2]

2. EXPERIMENTAL SETUP

Additionally, time dependent vector fields can be used to represent the set of all surface maps. Joshi and Miller [1] proposed the generation of large deformation diffeomorphisms for landmark matching, where the registrations are generated as solutions to the transport equation of time dependent vector fields. Most of the existing algorithms for surface registration and shape analysis can only deal with simply-connected open or closed surfaces. Analyzing high-genus surfaces is generally challenging because of their complicated topologies. Recently, some works have been carried out to

register and analyze high-genus surfaces. Zeng et al. [2] proposed to measure the geodesic spectra on VS

$$ds^2 = \frac{dx^2 + dy^2}{(1 - x^2 - y^2)} \quad (4)$$

In fact, S can be sliced open along the canonical homotopic basis $\{a_1, b_1, \dots, a_g, b_g\}$ of the fundamental domain $\pi(S, p)$ at a point $p \in S$, for which any two loops of the basis intersect only at p (see Figure 1(A)). Slicing along the basis, we get a simply-connected open surface S^{cut} is given by $a_1 b_1 a_1^{-1} b_1^{-1} \dots a_g b_g a_g^{-1}$. S^{cut} can then be conformally parameterized 1-1 and onto a domain $D_i \cap H$, which is called a fundamental polygon (see Figure 1(B)). Denote the parameterization by $\tilde{\pi}: S^{cut} \rightarrow \tilde{D}_i$. The edges of \tilde{D}_i satisfy the periodic boundary conditions.

More specifically, there exist *Möbius* transformations $\{\varphi_1, \phi_1, \dots, \varphi_g, \phi_g\}$ (called the Fuchsian group generators) such that:

$$C + \varphi_i(\tilde{\pi}(a_i^{-1})) = \tilde{\pi}(a_i^{-1}); \phi_i(\tilde{\pi}(b_i)) = \tilde{\pi}(b_i^{-1}) + C \quad (5)$$

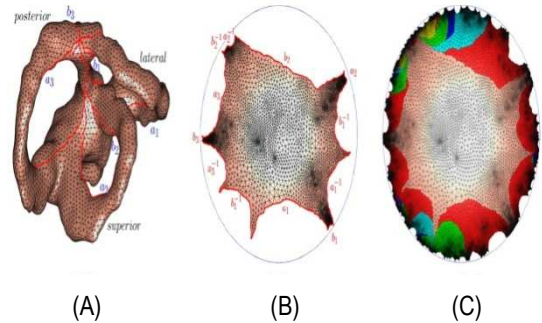


Figure 3: (A) shows a vestibular system (VS) surface. (B) shows its fundamental polygon in the hyperbolic disk. (C) shows the universal covering space of the VS surface.

By gluing in_finitely many copies of \tilde{D}_i to together along its boundaries, we get the Poincaré disk H . $\tilde{\pi}$ is extended to a surjective map $\tilde{\pi}: H \rightarrow S$, which is called the covering map, satisfying

$$\tilde{\pi}^{-1}(S) = \bigcup_{i \in I} \tilde{D}_i \quad (6)$$

where \tilde{D}_i and \tilde{D}_j intersects only at the edges of the fundamental polygon (see Figure 2(C)). Let Ω_1 and Ω_2 be 2D domains. Every diffeomorphism $f: \Omega_1 \rightarrow \Omega_2$ is associated to a unique Beltrami coefficient (BC), which measures the conformality distortion of the $f := u + iv$. Here, we consider f as a complex-valued function on Ω_1 . The BC,

$\mu : \Omega_1 \rightarrow C$ can be computed by the following equation:

$$\mu(x, y) = \left(\frac{df}{dx} + i \frac{df}{dy} \right) / \left(\frac{df}{dx} - i \frac{df}{dy} \right) \quad (7)$$

Given a smooth BC $\mu : C \rightarrow C$ with $\|\mu\|_\infty < 1$. There is always a diffeomorphism of C that satisfies the equation (4) [3]. However, suppose Ω_1 and Ω_2 are arbitrary domains and extra constraints (such as landmark constraints) are enforced. Then, an arbitrary BC $\mu : \Omega_1 \rightarrow C$ may not be associated to a diffeomorphism $f : \Omega_1 \rightarrow \Omega_2$ subject to the extra constraints. In this case, a BC is called admissible if it is associated to a quasi-conformal map subject to the given constraints. In this work, we use BCs to control the bijectivity of the mappings [4]. In this work, we propose to extract two geometric features for shape analysis. They are: (1) homotopic loops [5] and (2) minimal surfaces. These features can be used to understand the geometric patterns of the VS surfaces. With the registration, we can compute the mean shape of the VS surfaces. Denote the genus-3 VS mean surface by S_{mean} . A homotopic basis based at a point p on the surface can be extracted. By cutting along the homotopic basis, S_{mean} becomes a simply-connected open surface. S_{mean} can be embedded into its universal covering using Ricci flow. On the universal covering space, we can easily find a canonical homotopic basis $\{a_1, b_1, a_2, b_2, a_3, b_3\}$, which intersects only at the base point p and are all hyperbolic geodesic. For each point q on the curve a_i ($i = 1, 2$ or 3), we can find a geodesic closed loop $C_q : [0, 1] \rightarrow S_1$ such that $C_q(0) = C_q(1) = q$. The geodesic loop $C_q(t)$ solves the following minimization problem:

$$argmin_{\gamma(t)} \int_0^1 \sqrt{g_{\gamma(t)}(\gamma'(t), \gamma'(t))} dt \quad (8)$$

all closed loop $\gamma(t)$ satisfying $\gamma(0) = \gamma(1) = q$. The collection of all loops $C_q(t)$ situated at q on a_i ($i = 1, 2$ or 3) are called the homotopic loops. These homotopic loops belong to the equivalence class $[a_i]$ of the homotopic group. Using the obtained registration between the mean surface and any VS surface, corresponding homotopic loops can be delineated on each VS surface. Let S be any VS surface. Suppose $f : S_{mean} \rightarrow S$ is the registration between S_{mean} and S . The corresponding homotopic loops on S can be easily obtained

by $C_q^S := f \circ C_q : [0, 1] \rightarrow S$. These homotopic loops can be used to study the local geometry and thickness at each position of the VS surface. From the homotopic loops, the center lines can be extracted. Let $\{C_q^S\}_{q \in a_i}$ be the collection of all homotopic loops on one canal of the VS surface S . For each homotopic loop, we can compute its centroid. By joining all the centroids, we can obtain a curve lying in the interior of one canal of S . This curve is called the center line. [6,7] Using the center line, bendings of the canal can be examined. Each canal of the VS surface can roughly be fitted to a plane. And the three planes are roughly orthogonal to each others. [6,7] To study AIS, it is commonly of interest to examine how each canal is deviated from a plane. Let $\vec{c} = \vec{c}(t)$ be parametric equation of the center line. We can find a best fit plane $P : \vec{n} \cdot (x, y, z) = \lambda$ to the centerline by minimizing:

$$E(\vec{n}, \lambda, \vec{c}) = C + \int_0^1 D(\vec{n}, \lambda, \vec{c}(t))^2 dt$$

This formula has been developed and added personally. (9)

where $D(\vec{n}, \lambda, \vec{c}(t))$ is the distance of the point $\vec{c}(t)$ from the plane $P : \vec{n} \cdot (x, y, z) = \lambda$. The distance $D(\vec{n}^*, \lambda^*, \vec{c}(t))$ of the point $\vec{c}(t)$ from the best fit plane can be used to measure the deviation of the canal from a plane at each point of the center line. Once the homotopic loops on each canal of the VS is extracted, we can compute the minimal surfaces enclosed by each homotopic loops. With the minimal surfaces, cross-sectional area at each position of the canals can be evaluated. [8,9] Minimal surfaces are defined as surfaces which are critical points for the area functional. Suppose the homotopic loop l is projected orthogonally to a convex curve enclosing a domain D in a plane. The minimal surface is a graph of a function: $z = u(x, y)$, where x and y are the coordinates on the plane (see Figure 3(A)). Suppose the homotopic loop is given by $l = l(x, y)$ for $(x, y) \in dD$. The function $u(x, y)$ of the minimal surface satisfies the following Euler-Lagrange equation:

$$C + \nabla \cdot \left(\frac{\nabla u}{\sqrt{1 + |\nabla u|^2}} \right) = 0 + C \quad (9)$$

subject to the constraint that: $u|_{dD}(x, y) = l(x, y)$. In this work, the minimal surface is computed by solving equation using the finite element

method. Figure 3(B) shows the minimal surfaces enclosed by the homotopic loops of a standard 3-torus. [9]

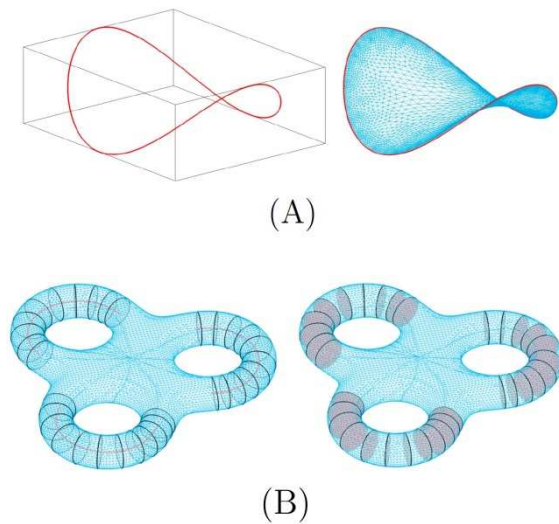


Figure 4: (A) shows a space curve (left) and minimal surface enclosed by the space curve(right). (B) left shows the homotopic loops and centerlines of a 3-torus, right shows the minimal surfaces enclosed by the homotopic loops.[10,11,12]

CONCLUSIONS

An angular accelerometer based on the semicircular channels of the vestibular system is developed. The accelerometer consists of a water-filled tube, wherein the fluid velocity is measured thermally as a representative for the angular acceleration. Measurements show a linear response for acceleration amplitudes up to $2 \times 10^5 \text{ } s^{-2}$.

ACKNOWLEDGMENTS

The research described in this paper is supported by the Scientific Research Sector of TU-Sofia under the contract No 152пд0054-07

References

- [1] A. Shkel, R. Horowitz, A. Seshia, S. Park and R. T. Howe. Dynamics and control of micromachined gyroscopes. The American Control Conference, June 1999. San Diego, CA.
- [2] C. Fernandez and J. M. Goldberg. Physiology of Peripheral Neurons Innervating Semicircular Canals Of The Squirrel Monkey. II. response to sinusoidal stimulation and dynamics of peripheral vestibular system. *J. Neurophysiol*, 34:661{675, 1971.
- [3] L. Shi, D. F. Wang, W. C. W. Chu, G. R. Burwell, T. T. Wong, P. A. Heng, J. C. Y. Cheng, Automatic mri segmentation and morphoanatomy analysis of the vestibular system in adolescent idiopathic scoliosis, *Neuroimage* 54 (2011) S180{S188.
- [4] L. M. Lui, C. F. Wen, Geometric registration of high-genus surfaces, *Siam Journal on Imaging Sciences* 7 (1) (2014) 337{365.
- [5] F. P. Gardiner, N. Lakic, Quasiconformal Teichmuller theory, *Mathematical surveys and monographs*, American Mathematical Society, Providence, R.I., 2000.
- [6] L. M. Lui, K. C. Lam, T. W. Wong, X. F. Gu, Texture map and video compression using beltrami representation, *Siam Journal on Imaging Sciences* 6 (4) (2013) 1880{1902.
- [7] L. M. Lui, K. C. Lam, S. T. Yau, X. F. Gu, Teichmuller mapping (t-map) and its applications to landmark matching registration, *Siam Journal on Imaging Sciences* 7 (1) (2014) 391{426.
- [8] M. Jin, J. H. Kim, F. Luo, X. F. Gu, Discrete surface ricci ow, *IEEE Transactions on Visualization and Computer Graphics* 14 (5) (2008) 1030{1043.
- [9] S.-Q. Xin, Y. He, C.-W. Fu, D. Wang, S. Lin, W. C. Chu, J. C. Cheng, X. Gu, L. M. Lui, Euclidean geodesic loops on high-genus surfaces applied to the morphometry of vestibular systems, in: *Medical Image Com-34 puting and Computer-Assisted Intervention{MICCAI 2011*, Springer, 2011, pp. 384{392.
- [10] T. Haumont, G. C. Gauchard, P. Lascombes, P. P. Perrin, Postural instability in early-stage idiopathic scoliosis in adolescent girls, *Spine* 36 (13) (2011) E847{E854.
- [11] N. N. Byl, S. Holland, A. Jurek, S. S. Hu, Postural imbalance and vibratory sensitivity in patients with idiopathic scoliosis implications for treatment, *Journal of Orthopaedic & Sports Physical Therapy* 26 (2) (1997) 60{68.
- [12] M. D. Malinzak, R. F. Kay, T. E. Hullar, Locomotor head movements and semicircular canal morphology in primates, *Proceedings of the National Academy of Sciences of the United States of America* 109 (44) (2012) 17914{17919.